Influence of Local Coercivity Variation on Magnetization Reversal Dynamics

Sug-Bong Choe, Hyuk-Jae Jang and Sung-Chul Shin

Department of Physics and Center for Nanospinics of Spintronic Materials,
Korea Advanced Institute of Science and Technology, Taejon 305-701, Korea

Local coercivity variation of Co/Pd nanomultilayers has been investigated by measuring the polar Kerr hysteresis loops of local areas of submicron size using a magnetooptic Kerr microscope system. Interestingly, the local coercivity distribution is very sensitive to an increase in the number of repeats: the (2-Å Co/11-Å Pd)$_{10}$ sample showed a smooth variation of the local coercivity, while (2-Å Co/11-Å Pd)$_{18}$ showed a large fluctuation. From micromagnetic considerations based on a thermally activated relaxation model, we have found that this local coercivity variation has a crucial effect on the contrasting magnetization reversal behavior observed in those samples: dominant wall-motion for the former sample and dominant nucleation for the latter one.

1. Introduction

Ultrathin ferromagnetic films and nanomultilayers are of great interest in recent years due to the possibilities of nanomagnetic applications, as well as their novel magnetic properties [1-4]. To achieve high performance in nanomagnetic applications it is necessary to prepare the materials nanoscopically uniform, since the irregularity and stability of domain formation are greatly affected by the nanomagnetic regularity of the film during the magnetization reversal process [5-9]. Much effort has been devoted to characterizing the nanomagnetic nature of the films by measuring topographic and magnetic images [10-13]. However, magnetization dynamics has rarely been studied by imaging techniques, because it has been difficult to apply external fields to samples in imaging systems. Recently, we have developed a local hysteresis loop measurement technique within the optical resolution limit by adopting a magnetooptic Kerr microscope system. In this study, we have investigated the local coercivity distribution of Co/Pd nanomultilayers having perpendicular anisotropy, by measuring the local hysteresis loops. The contrasting domain configuration and reversal behavior of the Co/Pd nanomultilayers reported by Choe and Shin [9] has been reexamined in accordance with the local coercivity distribution.

2. Experiments

A high-performance Kerr microscope system has been developed to measure the local hysteresis of magnetooptic thin films having perpendicular magnetic anisotropy [14, 15]. The system mainly consists of an polarizing optical microscope capable of 1,000× magnification with spatial resolution of 0.3 μm and Kerr angle resolution of 0.2°. To measure the hysteresis, the system is equipped with an electromagnet controlled by a personal computer to sweep the external magnetic field over the range of ±5 kOe.

The domain images are captured by an advanced CCD camera system which is interfaced to the computer. The images are composed of the light intensity distribution measured by a CCD array of 100×80 pixels, where a unit pixel corresponds to an area of 0.32×0.32 μm^2 at the film surface. Storing the domain images while sweeping the external magnetic field, it is possible to obtain an array of the local intensity function $I_{xy}(H)$. This is done by recording the intensity variation at every corresponding (x, y)th CCD pixel while sweeping the external field H. Figure 1(a) shows the typical dependence of the intensity variation on the applied magnetic field H. The intensity $I_{xy}(H)$ is correlated with the Kerr rotational angle $\theta_{xy}(H)$ by

$$I_{xy}(H) = I_{xy}^0 + C_{xy}\sin^2(\theta_{xy}(H) + \alpha_{xy}(H) + \Delta\theta_{xy}), \qquad (1)$$

where I_{xy}^0 is the intensity offset of the corresponding CCD pixel, C_{xy} is the proportionality coefficient between the intensity and the Kerr rotational angle, α_{xy} is the effective Faraday coefficient of the objective lens of the microscope, and $\Delta\theta_{xy}$ is the angle between the polarizer and the analyzer. Fitting the measured $I_{xy}(H)$ versus H to Eq. (1) for the two saturated states $\theta_{xy}(H) = \pm\theta_{xy}^M$ as shown by the solid lines in Figure 1(a), one can determine the values of I_{xy}^0, $(C_{xy}\alpha_{xy}^2)$, $(\Delta\theta_{xy}/\alpha_{xy})$, and $(\theta_{xy}^M/\alpha_{xy})$ with the approximation $\sin\theta \sim \theta$ for small θ. Then Eq. (1) can be rearranged as an explicit function for the normalized Kerr hysteresis loop in terms of the fitting parameters;
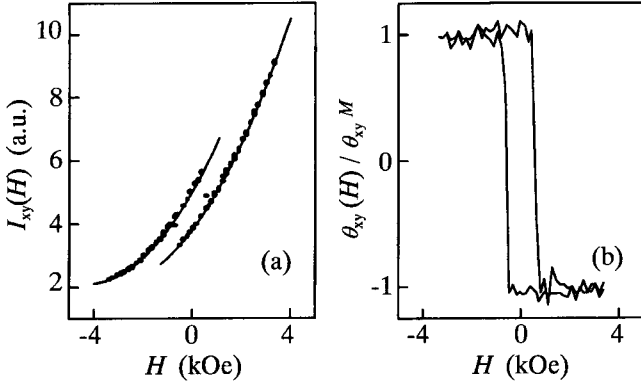
Fig. 1. (a) Typical value of the local intensity variation $I_{xy}(H)$ measured by the (x, y)th CCD pixel as a function of an applied magnetic field H. The solid lines are the fitting curves given by Eq. (1) for the two saturated states of $\theta_{xy}(H)=\pm\theta_{xy}^{M}$. (b) The normalized Kerr hysteresis loop $\theta_{xy}(H)$ generated from the intensity variation shown in (a).

$$\left(\frac{\theta_{xy}(H)}{\theta_{xy}^{M}}\right)=\left(\frac{\alpha_{xy}}{\theta_{xy}^{M}}\right)\left(\sqrt{\frac{I_{xy}(H)-I_{xy}^{0}}{C_{xy}\alpha_{xy}^{2}}}-H\right)-\left(\frac{\Delta\theta_{xy}}{\theta_{xy}^{M}}\right). \qquad (2)$$

Figure 1(b) shows the normalized Kerr hysteresis loop generated from the intensity variation shown in Figure 1(a). It should be stressed here that a Kerr hysteresis loop can be obtained for each CCD pixel, and thus one can generate a microscopic map of the local coercivity distribution H_C (x, y) by measuring the coercivity from the corresponding hysteresis loop of each CCD pixel at (x, y). The local coercivity distribution $H_C(x, y)$ is further deconvoluted by $H_C(x, y)=H_C^{0}+\delta H_C(x, y)$, where H_C^{0} is the mean value of the local coercivity and $\delta H_C(x, y)$ is the local variation of the coercivity.

3. Results and Discussion

The local coercivity distribution of Co/Pd nanomultilayers has been investigated in this way. Samples of (2-Å Co/ 11-Å Pd)$_n$ with varying number of repeats n were prepared on glass substrates by e-beam evaporation under a base pressure of 1.0×10^{-6} torr at ambient temperature. The nanomultilayered structure was achieved by alternatively exposing the substrate to two e-beam sources with typical deposition rates of 0.3 Å/s for Co and 0.5 Å/s for Pd. The layer thickness was controlled within 4% accuracy using real-time thickness measurement [14]. The samples of $n=$ 10 and 18 were extensively examined. Both samples had perpendicular magnetic anisotropy and showed square MH hysteresis loops. The coercivities measured by VSM were 1.3 and 2.4 kOe for the samples of $n=10$ and 18, respectively.

Interestingly, the local coercivity distribution was found to be very sensitive to the number of repeats n. In Figure 2, we illustrate the local coercivity distribution of (a) $n=10$ and (b) 18, respectively, by mapping $\delta H_C(x, y)$ in gray levels on a 2-dimensional XY plane, where the area of the maps corresponds to 32.8×26.2 μm^2 at the sample surface. It is surprising that the local coercivity distribution is so dependent on the number of repeats n: the thinner film with $n =$ 10 shows a smooth variation of the local coercivity as shown in Figure 2(a), while the thicker film with $n =18$ shows a large fluctuation of the local coercivity as shown in Figure 2(b). The standard deviation ΔH_C of the local coercivity distribution increased from 22 to 34 Oe with an increase in n from 10 to 18. The large fluctuation of the local coercivity of the thicker film is possibly ascribed to a larger amount of structural irregularity, because local structural irregularities such as atomic misfit, defects, and
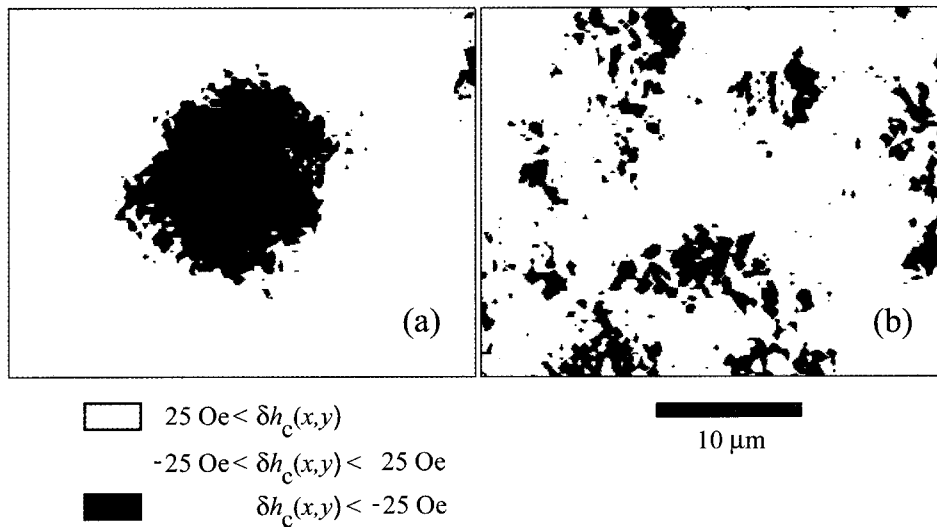

$\square$ $25\,\mathrm{Oe} < \delta h_c(x,y)$

$-25\,\mathrm{Oe} < \delta h_c(x,y) < 25\,\mathrm{Oe}$

$\blacksquare$ $\delta h_c(x,y) < -25\,\mathrm{Oe}$

$\blacksquare\blacksquare\blacksquare$
$10\,\mu m$

Fig. 2. The local coercivity distributions of (a) the (2-Å Co/11-Å Pd)$_{10}$ and (b) (2-Å Co/11-Å Pd)$_{18}$ samples. The total area of the map corresponds to the sample surface area of 32.8×26.2 μm^2. The map was generated by 100×80 coercivity measurements of individual pixels, each with area 0.32×0.32 μm^2.

20% REVERSAL

10 μm

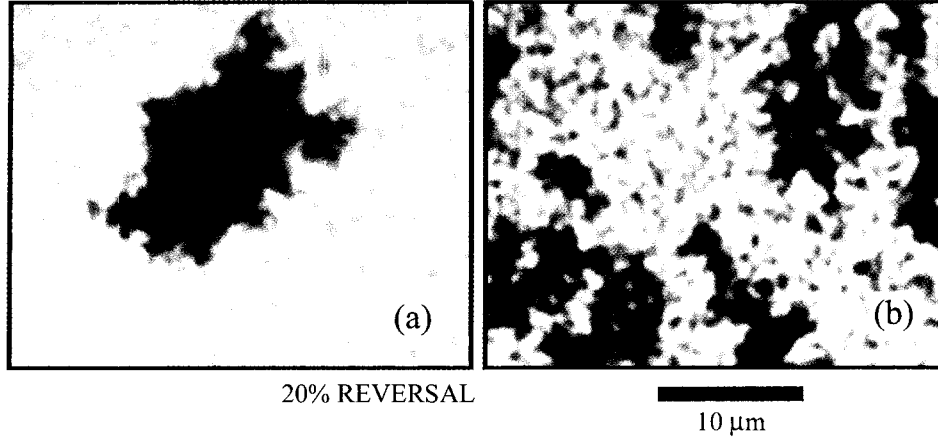Fig. 3. Typical domain patterns at 20% magnetization reversal from the saturated state for (a) (2-Å Co/11-Å Pd)$_{10}$ and (b) (2-Å Co/11-Å Pd)$_{18}$ samples.

dislocations, may be accumulative during film deposition. The local structural irregularity is known to cause magnetic inhomogeneity, such as misorientation of the polycrystalline axes, reduction of the nucleation field, and domain-wall pinning [16].

Magnetization reversal behavior of the Co/Pd nano-multilayer samples has been investigated by time-resolved observation of domain evolution from the saturated state under a reversed applied field [14, 15]. The reversal process in this system was found to change from dominant wall-motion to dominant nucleation with increasing number of repeats n. Figure 3 shows the typical domain patterns of the samples with (a) $n=10$ and (b) 18, respectively, during the magnetization reversal. The figures were grabbed from the same positions of the corresponding samples shown in Figure 2 using the same CCD camera attached to the microscope system and were subsequently intensified by noise filtering and brightness-contrast adjustment. The black regions in the figures are the reversed domains at 20% reversal from the saturated state. A large domain is clearly observed in Figure 3(a), while a number of small domains are seen in Figure 3(b). These contrasting reversal patterns occur by a balance between the nucleation process and the wall-motion process [7, 8]: he large domain shown in Figure 3(a) is formed by wall-motion process from a single nucleation site, while the small domains in Figure 3(b) are nucleated independently.

It is very interesting to note that these contrasting reversal patterns coincide with the local coercivity distributions. The reversal mechanism under conditions of local coercivity variation has been analyzed, based on a thermally activated relaxation process. The half-reversal time τ, which is the time needed to reverse half the volume of the sample, has been experimentally determined to decease exponentially with the applied field H [8]. By considering the local coercivity distribution $H_C(x, y)$, the half-reversal time $\tau(x, y)$ of magnetization M_S of a volume V_A located at (x, y) is given by

$$\tau(x, y) = \tau_0 \exp\left(\frac{V_A M_S}{k_B T}(H_C(x, y) - H)\right),\qquad(3)$$

where τ_0 is the characteristic reversal time for $H=H_C(x, y)$, k_B is the Boltzmann constant, and T is the temperature [7]. Then, the half-reversal time $\tau(x, y)$ is locally irregular even under a spatially-uniform applied field H, because $\tau(x, y)$ is proportional to the value of $\exp(V_A M_S \delta H_C(x, y)/k_B T)$. Since the magnetization reversal primarily happens in regions of faster $\tau(x, y)$ while the reversal process is impeded at the regions of slower $\tau(x, y)$, the domain reversal pattern is sensitive to the variation in local reversal time. As the local coercivity variation is increased, the wall-motion is pinned at the regions of slower reversal speed and the reversal proceeds by nucleation at regions of faster reversal speed, independently of the existing domains. This type of reversal behavior is perceived as a dominant nucleation reversal. On the other hand, the reversal behavior under a smooth coercivity distribution is dominated by the wall-motion overcoming the smaller wall-pinning effect.

By measuring the magnetization viscosity curves on changing the reversed applied field H, the values of $(V_A M_S/k_B T)$ were determined to be 3.0×10^{-2} Oe^{-1} and 2.5×10^{-2} Oe^{-1} for the samples with $n=10$ and 18, respectively and the reversal time variation $\exp(V_A M_S \Delta H_C/k_B T)$ was estimated to be 1.9 and 2.3 for the samples of $n=10$ and 18, respectively. Thus, it could be well explained that the reversal behavior of the sample with $n=10$ is dominant wall-motion with a smooth coercivity variation as shown in Figure 2(a), while the reversal of the sample with $n=18$ is dominant nucleation with a large coercivity fluctuation as shown in Figure 2(b).

To better understand the dependence of the reversal dynamics on the local coercivity variation, a theoretical study has been carried out by Monte Carlo simulation adopting a simple uniaxial anisotropy model [14, 17, 18]. In this model, the film is considered to be composed of nano-sized single domain cells on a hexagonal lattice lying in the XY plane, with periodic boundary conditions [19]. The vol-

ume V_c of a hexagonal unit cell is given by $\sqrt{3}t_f d_c^2/2$, where t_f is the film thickness and d_c is the distance between the centers of the nearest cells. Each cell has saturation magnetization M_s and uniaxial perpendicular anisotropy K_u, and each cell boundary has wall energy density σ_w. The magnetic energy E of a cell having magnetization making an angle θ with the $+z$ axis is given by

$$E=K_u V_c \sin^2\theta - M_s V_c(H_z + H_d)\cos\theta$$
$$+\left(3 - \frac{1}{2}\cos\theta\sum_k \cos\theta_k\right)\frac{d_c t_f \sigma_w}{\sqrt{3}}, \qquad (4)$$

where the first term is the uniaxial anisotropy energy, the second term is the magnetostatic energy due to both the external field H_z and the demagnetizing field H_d normal to the film, and the last term is the domain-wall energy summed over the six boundaries with the nearest neighbor cells having the magnetization direction θ_k. The demagnetizing field H_d acting on the cell is calculated by summing the magnetostatic field from the magnetization of the neighboring cells out to the Nth nearest cells, by considering the magnetostatic interaction energy between the surface magnetization distribution of the cells. We took $N=40$, where H_d was almost saturated to its asymptotic value [19].

The magnetic energy E has two minima, at $\theta=0$ and π, with a maximum in between. The energy barrier to reversal, E_B, is the difference in energy between the initial value and the maximum, and it is given by

$$E_B=K_u V_c\left[1 + \cos\theta\frac{M_s(H_z + H_d) + (\sigma_w/3d_c)\Sigma_k\cos\theta_k}{2K_u}\right]^2,$$
$$\qquad (5)$$

where θ and θ_k are the initial magnetization direction of the cell and the nearest neighbors, respectively. The probability P of a cell reversing through the energy barrier E_B by thermally activated fluctuation in time Δt is

$$P=P_0 \exp(-E_B/k_B T)\Delta t, \qquad (6)$$

where P_0 is the probability constant, k_B is Boltzmann's constant, and T is the temperature. The value $P_0\Delta t$ is determined to make $\Sigma_{x,y} P(x, y)=1$ by a preliminary calculation of $P/P_0\Delta t$ over the whole sample. A cell is determined to be reversed when a random value ranging [0, 1] is greater than the probability P of cell reversal and then, the total domain pattern is constructed from the state of each individual cell.

Magnetization reversal of the Co/Pd nanomultilayers has been investigated by this simulation algorithm. To investigate the influence of structural nonuniformity, we assigned a random fluctuation to the uniaxial perpendicular anisotropy of each cell, where the fluctuation function was chosen to have a Gaussian distribution and the other magnetic properties held constant for every cell in the sample. The perpendicular magnetic anisotropy, rather than the saturation magnetization, is expected to be very sensitive to structural irregularity in this system, since it is mainly caused by the structurally-induced anisotropy at interfaces. Typical values of the magnetic properties of the Co/Pd nanomultilayered system were used in the simulation: uniaxial anisotropy $K_U=1\times10^6$ erg/cm^3, saturation magnetization $M_S=250$ emu/cm^3, wall energy density $\sigma_W=0.8$ erg/cm^2, and cell volume $V_C=6.9\times10^{-18}$ cm^3.

Figure 4 shows the simulated domain patterns at 50% reversal with increasing anisotropy fluctuations of (a) 0, (b) 2, and (c) 4%, respectively. The domain patterns change from a large regular domain to a number of ragged domains as the anisotropy fluctuation increases. It is very interesting to note that these contrasting domain patterns are truly matched to the experimentally observed domain patterns: the large domain is formed by a wall-motion process from a single nucleation site, while the small ragged domains are nucleated by a nucleation process. The number of nucleation sites increases with an increasing number of repeats, which is ascribed to the increment of local coercivity fluctuation. It should be pointed out that the domain boundary is rougher in the thicker sample, which shows the existence of local structural irregularity. Considering the fact that the theoretical prediction was obtained by assuming identical values of the magnetic properties except for the local anisotropy distribution, the good correspondence between the experimental observation and the theoretical prediction implies an essential role of the local anisotropy variation on the domain reversal mechanism. For a sample with a large local anisotropy fluctuation, the reversal is initiated at sev-
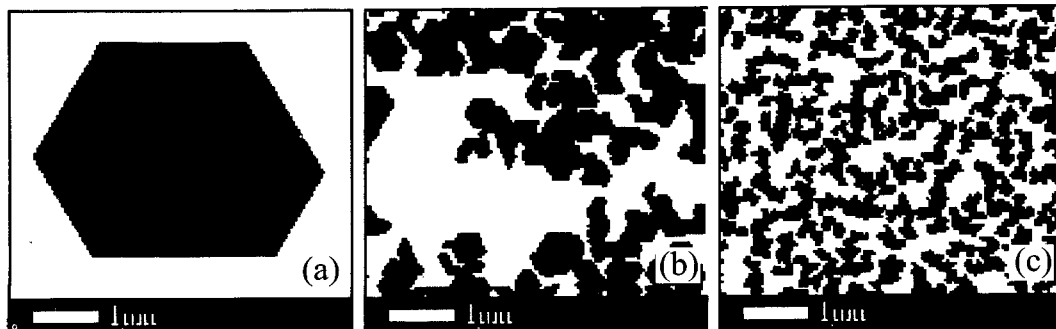

Fig. 4. Simulated domain patterns at 50% reversal for anisotropy variations of (a) 0%, (b) 2%, and (c) 4%, respectively.

eral nucleation sites of lower nucleation barrier energy and then the wall expansion from the nucleation sites is constrained at pinning sites with locally high energy barriers. Thus, several small domains with irregular boundaries appear as shown in Figure 4(c). On the other hand, a smooth anisotropy distribution has few nucleation sites and a weak pinning effect and thus, the reversal expands smoothly from one nucleated site by wall motion overcoming the pinning sites, as shown in Figure 4(a).

4. Conclusion

We have investigated the local coercivity distribution of Co/Pd nanomultilayers having perpendicular anisotropy, by measuring the local hysteresis loops of local areas of submicron size using a magnetooptic Kerr microscope system. The local coercivity distribution was very greatly increased with increasing number of repeats: the $(2\text{-Å Co/11-Å Pd})_{10}$ sample showed a smooth variation of the local coercivity, while $(2\text{-Å Co/11-Å Pd})_{18}$ showed a large fluctuation. From a micromagnetic argument based on a thermally activated relaxation model, we have found that this local coercivity variation had a crucial effect on the contrasting magnetization reversal behavior observed in those samples; dominant wall-motion for the former sample and dominant nucleation for the latter one.

Acknowledgments

References

[1] P. F. Carcia, A. D. Meinhaldt and A. Suna, Appl. Phys. Lett., **47**, 178 (1985).

[2] D. G. Stinston and S.-C. Shin, J. Appl. Phys., **67**, 4459 (1990).

[3] S.-C. Shin, Appl. Surf. Sci., **65**, 110 (1993).

[4] F. J. Himpsel, J. E. Ortega, G. J. Mankey and A. F. Willis, Adv. Phys., **47**, 511 (1998).

[5] H.-P. D. Shieh and M. H. Kryder, IEEE Trans. Magn., **24**, 2464 (1988).

[6] C.-J. Lin, J. C. Suits and R. H. Geiss, J. Appl. Phys., **63**, 3835 (1988).

[7] J. Pommier, P. Meyer, G. Pónissard, J. Ferré, P. Bruno and D. Renard, Phys. Rev. Lett., **65**, 2054 (1990).

[8] M. Labrune, S. Andrieu, F. Rio and P. Bernstein, J. Magn. Magn. Mater., **80**, 211 (1989).

[9] S.-B. Choe and S.-C. Shin, J. Appl. Phys., **83**, 6952 (1998); **85**, 5651 (1999).

[10] E. Dan Dahlberg and J.-G. Zhu, Phys. Today **48**, 34 (1995).

[11] M. R. Scheinfein, J. Unguris, M. H. Kelley, D. T. Pierce and R. J. Celotta, Rev. Sci. Instrum, **61**, 2501 (1990).

[12] E. Bauer, Rep. Prog. Phys., **57**, 895 (1994).

[13] E. Betzig, J. K. Trauman, R. Wolfe, E. M. Gyorgy, P. L. Finn, M. H. Kryder and C.-H. Chang, Appl. Phys. Lett, **61**, 142 (1992).

[14] S.-B. Choe and S.-C. Shin, Phys. Rev. B, **57**, 1085 (1998); J. Appl. Phys., **81**, 5743 (1997).

[15] S.-B. Choe and S.-C. Shin, Appl. Phys. Lett., **70**, 3612 (1997).

[16] H. Kronmüller, Phys. Stat. Sol. (b) **144**, 385 (1987).

[17] R. D. Kirby, J. X. Shen, R. J. Hardy and D. J. Sellmyer, Phys. Rev. B **49**, 10810 (1994).

[18] A. Lyberatos, J. Earl and R. W. Chantrell, Phys. Rev. B **53**, 5493 (1996).

[19] M. Mansuripur, J. Appl. Phys., **66**, 3731 (1989); **61**, 1580 (1987).